Acta Metallurgica Sinica (English Letters) (2021) 34:1483–1491
https://doi.org/10.1007/s40195-021-01325-y

Nature of CoCrFeMnNi/Fe and CoCrFeMnNi/Al Solid/Solid Interface

Zhongtao Li[1] · Weidong Zhang[1] · Zhenggang Wu[1,2]

Received: 9 August 2021 / Accepted: 5 September 2021 / Published online: 10 October 2021

Abstract
To shed light into the application potential of high-entropy alloys as "interlayer" materials for Al-steel solid-state joining, we investigated the nature of the CoCrFeMnNi/Fe and CoCrFeMnNi/Al solid/solid interfaces, focusing on the bonding behavior and phase components. Good metallurgical bonding without the formation of hard and brittle IMC can be achieved for CoCrFeMnNi/Fe solid/solid interface. In contrast to the formation of Al_5Fe_2 phase at the Fe/Al interface, $Al_{13}Fe_4$-type IMC, in which the Fe site is co-occupied equally by Co, Cr, Fe, Mn and Ni, dominates the CoCrFeMnNi/Al interface. Although the formation of IMC at the CoCrFeMnNi/Al interface is not avoidable, the thickness and hardness of the $Al_{13}(CoCrFeMnNi)_4$ phase formed at the CoCrFeMnNi/Al interface are significantly lower than the Al_5Fe_2 phase formed at the Fe/Al interface. The activation energies for the interdiffusion of Fe/Al and CoCrFeMnNi/Al static diffusion couple are 341.6 kJ/mol and 329.5 kJ/mol, respectively. Despite this similarity, under identical static annealing condition, the interdiffusion coefficient of the CoCrFeMnNi/Al diffusion couple is significantly lower than that of the Fe/Al diffusion couple. This is thus mainly a result of the reduced atomic mobility/diffusivity caused by the compositional complexity in CoCrFeMnNi high-entropy alloy.

Keywords High-entropy alloy · Microstructure · Metallurgical bonding · Interface

1 Introduction

A key and promising "weight-lightening" technology in transportation system is to blend the attractive properties of iron (Fe)-based steels and aluminum (Al) alloys in one hybrid part. This hybrid design makes the development and employment of effective Al-steel dissimilar metal joining methods of great interests. High-quality Al-steel welds using traditional fusion welding methods was found difficult to obtain, owing to the pronounced differences in thermophysical properties (e.g., melting points, thermal expansion coefficient and thermal and electrical conductivities) between Al alloys and steels [1–5]. Therefore, solid-state techniques were used or are under development with the hope of achieving the best quality of Al-steel welds, such as continuous and spot friction stir welding [6–9].

The major barrier to achieving high-quality solid-state Al-steel welds is the tendency to form inherently brittle intermetallic compounds (IMCs, mainly Al_3Fe, Al_5Fe_2, $Al_{13}Fe_4$) at the metallurgical bonding interface. The formation of IMCs could cause significant mechanical property degradation of the welds [10, 11]. Thus, great efforts were made with the hope of suppressing the IMC formation. The effectiveness of welding parameter (e.g., welding speed, power) adjustment was limited due to the intrinsic natures between Al and Fe: high chemical affinity and low Fe solubility in Al matrix. An intuitively more effective method would be avoiding the direct contact between the two diffusion medium, Al and Fe. Thus, "interlayer" between Al and steels was applied by a number of researchers. So far, the most widely used "interlayer" materials were mainly pure elemental materials. For example, Reddy et al. [12] investigated the effects of electroplating Ni, Cu and Ag on the continuous drive friction welding of AA6061 and AISI 304 steel. When Ag coating was applied on the steel fay surface, relatively less-brittle IMCs, Ag_2Al and FeAl, replaced Fe_5Al_2 and $FeAl_3$ at the bonding interface. Cu and Ni "interlayer" reduced the amount of Fe_5Al_2, but new brittle IMCs formed, including

Available online at http://link.springer.com/journal/40195

✉ Zhenggang Wu
zwu9@hnu.edu.cn

[1] College of Materials Science and Engineering, Hunan University, Changsha 410082, China

[2] State Key Laboratory of Advanced Design and Manufacturing for Vehicle Body, Hunan University, Changsha 410082, China

$CuAl_2$, CuAl, Al_3Ni and AlNi. The inevitability to form thick new IMCs is one of the common drawbacks of the typically used elemental "interlayer" materials. This made the weld-quality improvement still not optimal. Thus, a new type of "interlayer" material which can effectively reduce the IMC thickness and brittleness or eliminate the IMC layer(s) is urgently needed.

Recently, a new class of alloy, high-entropy alloy (HEA) [13–29], emerged in physical metallurgist's and alloy designer's world. HEAs, made of four or more elements with equi- or near-equiatomic ratio, exhibit four core effects [13, 22, 30–34], namely high-entropy effects, lattice distortion effects, sluggish diffusion effects and cocktail effects. The high-entropy effect of HEAs makes their microstructure preferentially dominated by solid solution. This combines with the sluggish diffusion effect, theoretically, makes HEAs exhibit great structural stability when external elements diffused into them through solid-state processes. Supporting findings are from a number of research groups when they were investigating the effectiveness of using HEA particles as reinforcement in metal matrix (MM). For example, Karthik et al. [35] additively manufactured an Al matrix composites reinforced with CoCrFeNi particles; at the particle/matrix interface, the high-entropy (solid solution) character of HEA particles was not loosened, microstructurally no brittle IMCs were observed. The absence of IMCs at HEA particle/MM interface was also observed by Lu et al. [36], Meng et al. [37] and Chen et al. [38] when compositionally different HEA particles (e.g., $CoNiFeAl_{0.4}Ti_{0.6}Cr_{0.5}$ and AlCoCrCuFeNi) were used as reinforcements to different metal matrixes (e.g., SiCp/7075Al and AZ91D).

The synergy of HEAs' high-entropy effects and sluggish diffusion effects makes them potential desirable candidates for "interlayer" materials during Al-steel solid-state joining. As Fig. 1 shows, while applying the HEA "Interlayer," the first step is normally to deposit a layer of HEA coating on steel substrate, followed by stacking Al alloys on the "interlayer." Then, the "sandwiched" *steel-HEA-Al* structure is solid-state welded (e.g., friction stir welded). Thus, in order to evaluate the possibility to use HEAs as Al-steel dissimilar metal joining "interlayer," we are conducting a series of studies to consecutively assess the behavior of the steel-HEA and Al alloy-HEA interface under static diffusion conditions and the behavior of steel-HEA-Al "sandwiched" stack under dynamic thermomechanical (i.e., welding) processes.

In this study, as the first trial, we assessed the potential to use the quinary "Cantor's alloy" [39–42] (equiatomic CoCrFeMnNi alloy) as the "interlayer" through extensive characterizations of the nature of the CoCrFeMnNi/Fe and the CoCrFeMnNi/Al solid/solid interfaces. The microstructure of the CoCrFeMnNi/Fe metallurgical bonding interface when CoCrFeMnNi was coated on the Fe substrate was firstly reported. Fe, the primary constituent element of steel, was chosen as the substrate to circumvent the complicated effects from other alloying elements that exist in steels. Next, the metallurgical bonding behavior of CoCrFeMnNi/Al interface was assessed; for the same reason, Al instead of Al alloys was used, and in this step, the microstructure of the Fe/Al interface was investigated for comparison purpose. The present study was taken up mainly to answer a few fundamental questions: will IMC form at the HEA/Fe solid-state interface? Can high-entropy effects of HEA prevent the formation of hard and brittle IMC layer at the CoCrFeMnNi/Al solid-state interface? Can the sluggish diffusion of HEA lead to the reduction in the IMC layer thickness? In addition to these, the kinetic behavior of the diffusion at the CoCrFeMnNi/Al interface will also be investigated to shed further insights.

2 Experimental

As schematically shown in Fig. 2, spark plasma sintering (SPS) technique (Sinter Land LABOX-325R) was used to consecutively generate the CoCrFeMnNi/Fe, CoCrFeMnNi/Al and Fe/Al solid/solid interfaces. First, pure Fe substrate was placed in a graphite die, and spherical CoCrFeMnNi powders (30 μm, obtained using gas atomization method) were placed on top of the substrate (Step 1). A pulse current was subsequently applied, while the die was maintained under of a uniaxial pressure of 30 MPa, leading to Joule heating among powder particles and the substrate to promote simultaneous powder sintering and particle–substrate metallurgical bonding under argon atmosphere. The interface

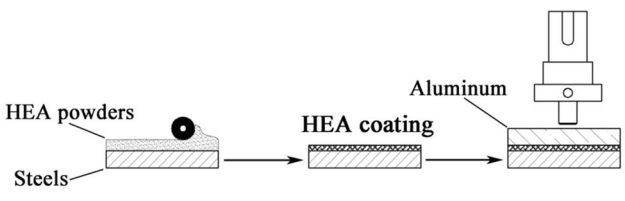

Fig. 1 Flowchart showing the typical procedure to apply HEA as Al-steel solid-state joining "interlayer" material, taking friction stir joining as an example

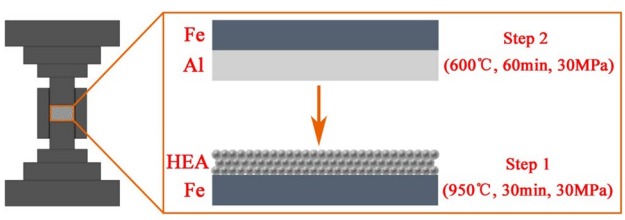

Fig. 2 Schematic showing the coating of CoCrFeMnNi on the Fe substrate and the diffusion bonding of Al with CoCrFeMnNi

was heated up to 950 °C with a heating rate of 100 °C/min and a soaking time of 30 min, followed by furnace cooling. After fulfilling the coating of HEA on Fe substrate, a piece of Al was placed on top of the HEA layers, and a piece of Fe was placed on top of the Al piece (Step 2). Then, the Fe-CoCrFeMnNi-Al–Fe stacking was heated up to 600 °C with a soaking time of 60 min. To compare the kinetic behavior of diffusion at the CoCrFeMnNi/Al and Fe/Al interfaces, a piece of Al was sandwiched between pieces of CoCrFeMnNi and Fe. The sandwiched structure was heated up to a variety of temperatures (550–625 °C) with different soaking time (15–60 min). The temperature was measured using a k-type thermocouple inserted near the inside diameter of the die.

Microstructures of the interfaces were characterized using a Quanta 650 FEG SEM coupled with energy dispersive spectrometer (EDS) and operated in the backscattered electron (BSE) mode. Electron backscatter diffraction (EBSD) measurements were performed at an accelerating voltage of 30 kV and a step size of 0.7 μm in a field-emission scanning electron microscope (FESEM; FEI XL30S, FEI Company). In addition, phase components at the interfaces were crystallographically examined using X-ray diffraction (XRD, Panalytical XPert PRO MRD goniometer) with a Cu $K\alpha$ radiation operating at 40 kV and 40 mA. The nanohardness of the interfaces was determined using a nanoindentation hardness tester (Micro Scratch Tester; MCT + UNHT, Swiss CSM company); the maximum load for the tests was 50 mN with loading rate of 10 mN/s, and the dwell time at the target load was 10 s.

3 Results and Discussion

The macrostructure of the generated Fe-CoCrFeMnNi-Al–Fe stacking is shown in Fig. 3. Simultaneous consolidation of CoCrFeMnNi powders and coating of the alloy on the Fe substrate was successfully achieved. The sintered CoCrFeMnNi alloy consists of equiaxed grains with an average grain size of 9 μm. From this low-magnification back-scatted electron (BSE) image, the pure Fe substrate and the simultaneously consolidated CoCrFeMnNi show good metallurgical bonding without clear reaction layer. In contrast, reaction layers with different thickness are visible at the CoCrFeMnNi/Al and Fe/Al interfaces.

3.1 Microstructure of the CoCrFeMnNi/Fe Interface

Figure 4a, b presents high-magnification BSE images for the CoCrFeMnNi/Fe interface, in which a thin transition layer was visible. A gradual instead of sharp composition transition across the CoCrFeMnNi/Fe boundary is shown in Fig. 4c, indicating the occurrence of a continuous diffusion. The transition layer composed mainly of Fe with minor addition Co, Cr, Ni and Mn. Quantitatively, this CoCrFeMnNi/Fe interface layer consists of 88.5 at.% Fe, 5.1 at.% Mn, 4.1 at.% Cr, 1.6 at.% Ni, and 0.7 at.% Co.

Previous HEA-related researches have summarized a few mixing-enthalpy-based, atomic-size-based, and mixing-entropy-based parameters (ΔH_{mix}, δ, and ΔS_{mix}, respectively) for the prediction of the dominant phase (single or multi-phase). Following these, from the interface composition, we calculated the value of ΔH_{mix} (0.32 kJ/mol), δ (1.916%) and ΔS_{mix} (1.61R) for the CoCrFeMnNi/Fe interface layer, and found that all of these meet the criteria (-15 kJ/mol $< \Delta H_{mix} < 5$ kJ/mol, $1\% < \delta < 6.6\%$ and $\Delta S_{mix} \geq 1.5$R) for forming single-phase solid solution alloy. This is a strong indication that the transition layer is a type of Fe-rich single-phase solid solution. This speculation was confirmed using EBSD (Fig. 5). Specifically, the inverse pole figure (IPF) in Fig. 5a shows that the transition region contained a layer of elongated grains along the interface boundary, which are identified as BCC phase (Fig. 5b). These findings lead us to conclude that during high-temperature sintering process, due to the compositional gradient, Co,

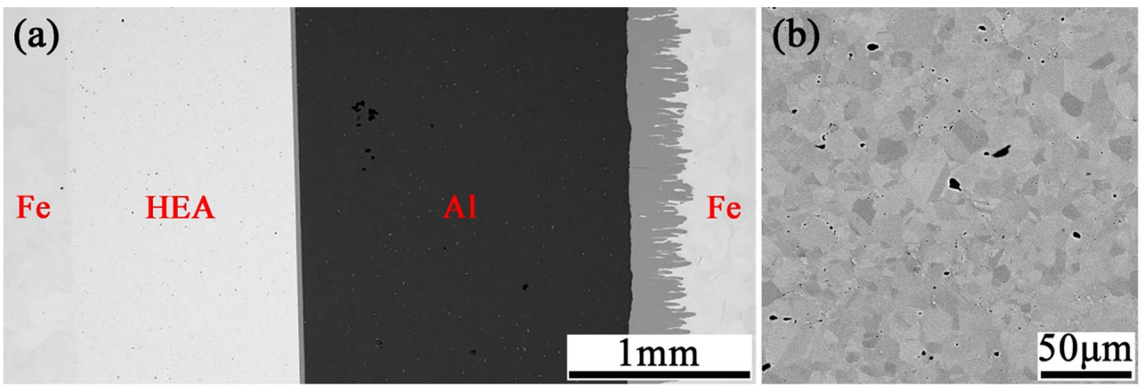

Fig. 3 **a** Macrostructure of the generated Fe-CoCrFeMnNi-Al–Fe stacking; **b** BSE image of the CoCrFeMnNi layer obtained through the simultaneous sintering and coating

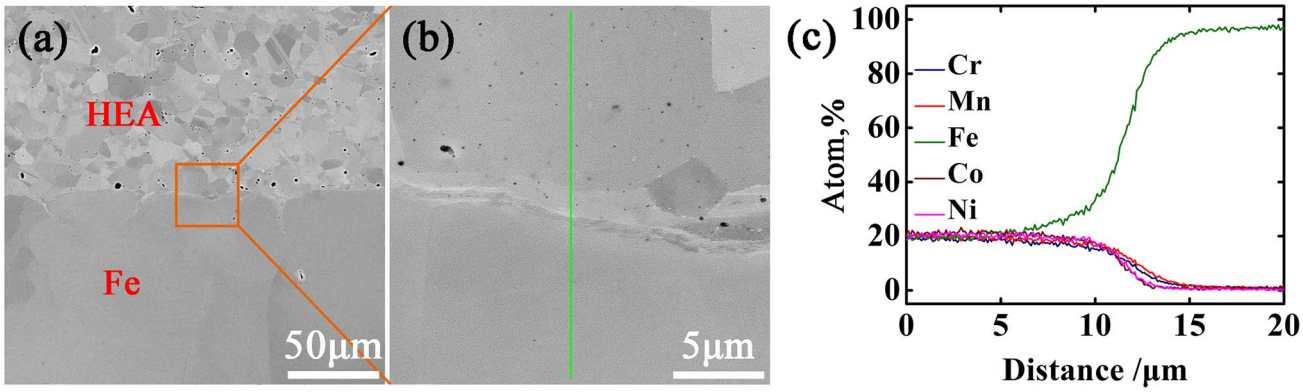

Fig. 4 **a** Macrostructure and **b** microstructure of the as-obtained CoCrFeMnNi/Fe interface and **c** the elemental distribution across the CoCrFeMnNi/Fe interface

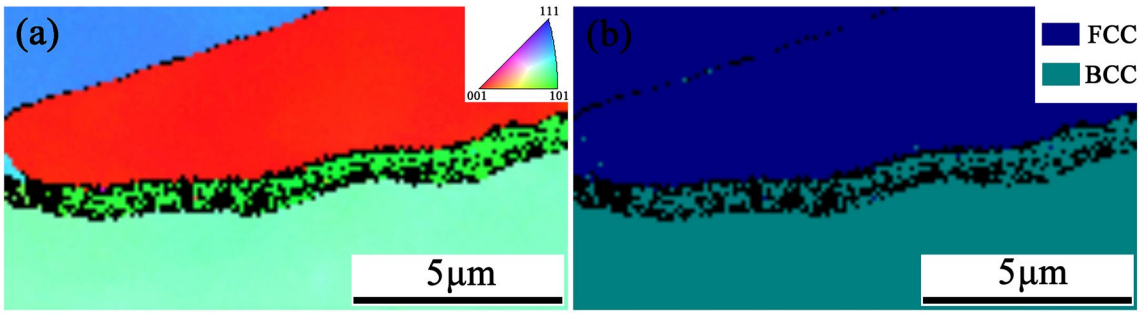

Fig. 5 EBSD images showing **a** the IPF pole figure and **b** the phase map of the as-obtained CoCrFeMnNi/Fe interface

Cr, Mn and Ni diffuse into the boundary grains with different diffusion coefficients; this leads to the as-observed composition change, which is not significant enough to cause phase change of the boundary grains.

3.2 Microstructure of the Fe/Al and CoCrFeMnNi/Al Interface

The macrostructure of the CoCrFeMnNi-Al–Fe stacking and the magnified views showing the two interfaces are shown in Fig. 6a–c. It is clear that both interfaces achieve good metallurgical bonding. Immediate differences that can be derived from the microstructure of the CoCrFeMnNi/Al and Fe/Al interfaces are the morphology and thickness of their reaction layers. Under the specific applied condition (600 °C, 60 min, 30 MPa), the Fe/Al interface has a tongue-like morphology and an average thickness of ~ 300 μm. The CoCrFeMnNi/Al interface is visually composed of three distinct layers and has an uniform thickness of ~ 25 μm. Another striking feature is that a few fine perpendicular cracks are visible at the Fe/Al interface, and the CoCrFeMnNi/Al interface is crack-free. Figure 6d, e shows the elemental distribution across the Fe/Al interface and the CoCrFeMnNi/Al interface, respectively. The composition across both interfaces does not display a significant fluctuation. Quantitatively, the Fe/Al interface layer contains ~ 71.4 at.% Al and 28.6 at.% Fe; the CoCrFeMnNi/Al interface layer is composed of 78 at.% Al with the remaining equally split by Co, Cr, Fe, Mn and Ni.

In order to determine the phase(s) of the interface reactions layers, selected area XRD was performed, and the obtained patterns are shown in Fig. 7. A complex pattern containing numerous peaks is observed for the Fe/Al interface. A careful analysis suggests that the pattern is composed of three sets of peaks, corresponding to the Al matrix, Fe matrix and Al_5Fe_2 IMC phase, respectively. Thus, we can assert that upon the solid/solid diffusion, Al_5Fe_2 phase forms at the Fe/Al interface. The nature (e.g., phase component, grain morphology) of the Fe/Al interface reaction product was further revealed using EBSD. As shown in Fig. 8a, the Fe/Al interface IMC layer consists of perpendicularly elongated grains which were confirmed to be dominated by a Al_5Fe_2-type IMC (Fig. 8b).

According to the binary Al–Fe phase diagram, a few types of IMC, Al_3Fe, Al_2Fe, FeAl as well as Al_5Fe_2 are thermodynamically stable at the 600 °C temperature [43]. The presence of only Al_5Fe_2 is a result of the fact that kinetically, the nucleation and growth of Al_3Fe, Al_2Fe and FeAl are too slow for them to grow to a visible thickness with the current

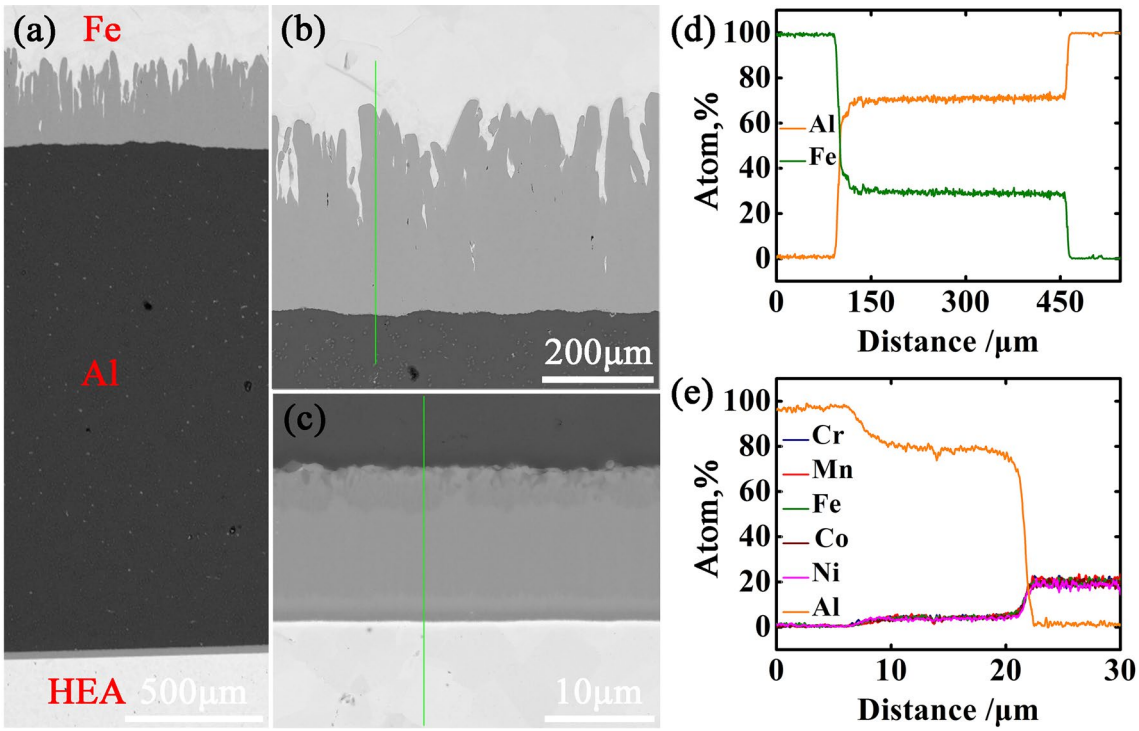

Fig. 6 **a** An overall view of the Fe-Al-CoCrFeMnNi sandwiched structure; magnified views of the obtained **b** Fe/Al interface and **c** CoCrFeMnNi/Al interface, the elemental distribution of which are presented in **d e**, respectively

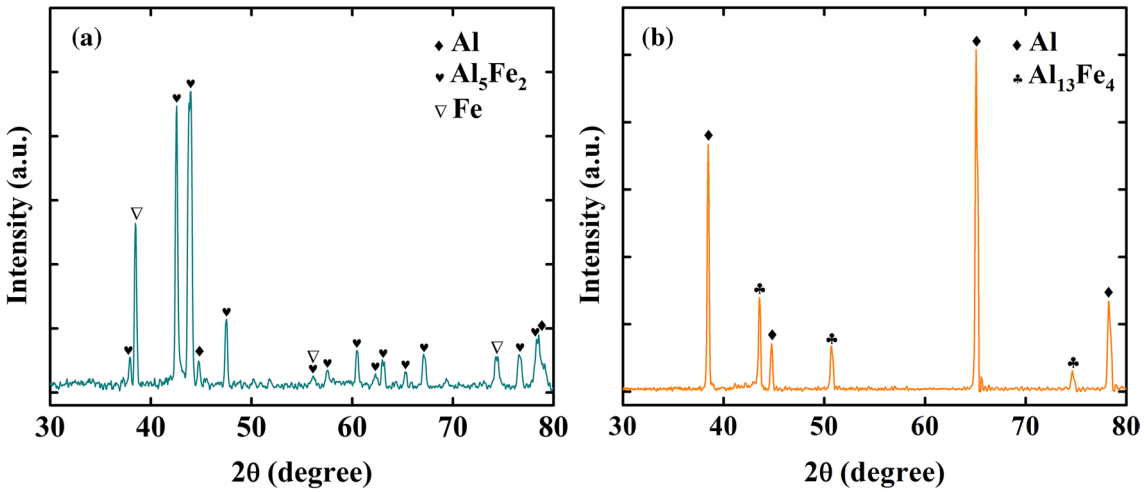

Fig. 7 Selected area XRD patterns of **a** the Fe/Al interface and **b** the CoCrFeMnNi/Al interface

experimental annealing time [44]. Under solid/solid Fe/Al interdiffusion, the self-diffusion coefficient of Fe in Al is significantly higher than that of Al in Fe [45]. Thus, it is generally recognized that the formation of IMC layer at the Fe/Al interface is dominated by the diffusion of Fe into the Al matrix [45]. Therefore, a type of Al-rich phase, $Al_{13}Fe_4$, which was not listed in the binary Al–Fe phase diagram, was very often found the first phase formed preceding the formation of the Fe-rich Al_5Fe_2 phase at the interface [10, 44]. As the continuous diffusing-into of Fe, the $Al_{13}Fe_4$ phase is gradually replaced by the Fe-rich Al_5Fe_2 phase. Most studies have shown that the dominant phase obtained during Fe/Al solid/solid interdiffusion is the Al_5Fe_2 phase, and occasionally, a thin $Al_{13}Fe_4$ layer was found between the Al_5Fe_2

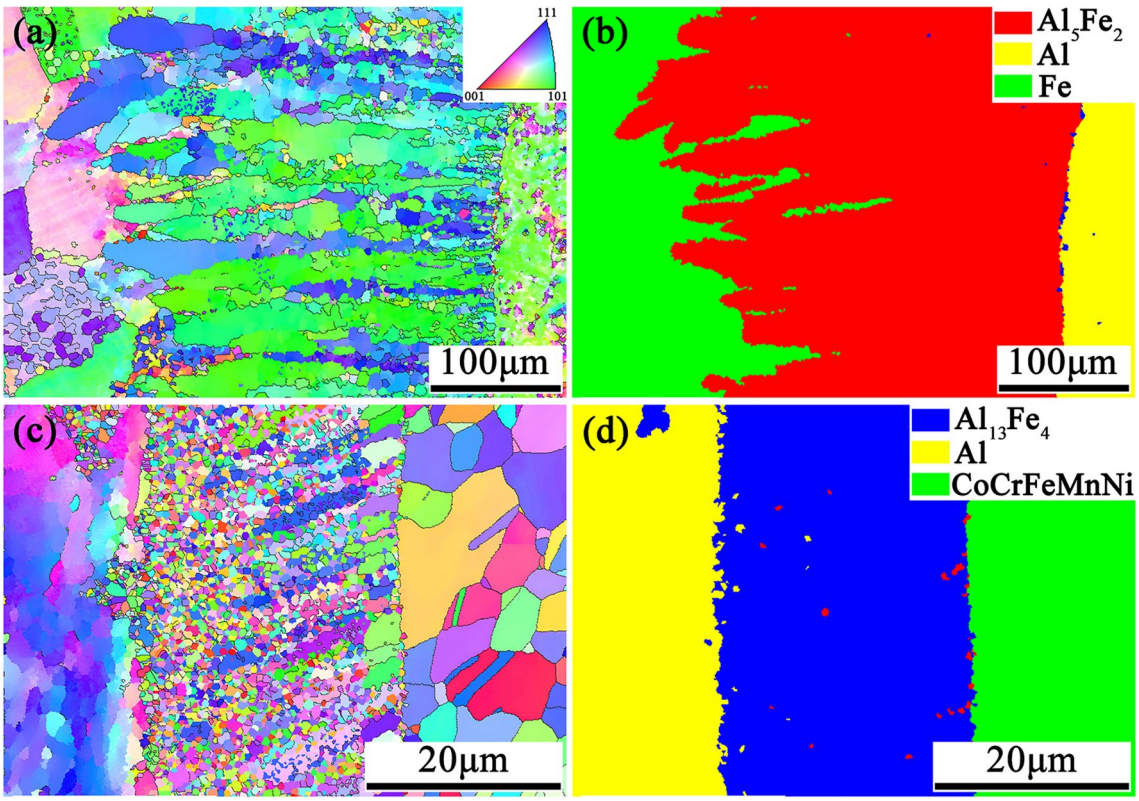

Fig. 8 EBSD images showing **a**, **c** the inverse pole figure images **b**, **d** the phase mappings of the as-obtained Fe/Al and CoCrFeMnNi/Al interfaces, respectively

phase and Al [41]. In the current study, the initially formed $Al_{13}Fe_4$ phase was completely replaced by the Al_5Fe_2 phase due to the high processing temperature and extended length of holding time. This observation is consistent with previous reports which showed the formation of a pure Al_5Fe_2 layer during solid/solid Al–Fe interdiffusion [10].

For the CoCrFeMnNi/Al interface, only major peaks (Fig. 7b) corresponding to the two matrices (Al and CoCrFeMnNi) can be seen. The failure to reveal the peaks corresponding to the reaction layer is due possibly to the relatively much lower thickness (~25 μm) of the layer compared to the scan diameter (~300 μm). The EBSD images show that at the CoCrFeMnNi/Al interface, the IMC layer mainly consists of equiaxed grains (Fig. 8c). In terms of the phase component, an $Al_{13}Fe_4$-type phase was found being the dominant, and the major differences of the three visually existent layers (Fig. 6c) at this interface are related to their grain sizes and grain morphology differences. The diffusion coefficient of Co, Cr, Fe, Mn and Ni in Al [46–48] at 600 °C are 9.71×10^{-16} m^2/s, 4.03×10^{-15} m^2/s, 1.43×10^{-16} m^2/s, 3.40×10^{-15} m^2/s and 2.90×10^{-16} m^2/s, respectively. If the same dominant process (the CoCrFeMnNi constituent elements diffuse into Al matrix) occurs at the CoCrFeMnNi/Al interface, a large difference in the amount of Co, Cr, Fe, Mn and Ni at the IMC layer would be expected. But surprisingly, the constituent elements of the CoCrFeMnNi alloy in the $Al_{13}Fe_4$ phase maintain their equiatomicity nature; this indicates that the original Fe site in the $Al_{13}Fe_4$ phase is now co-occupied equally by Co, Cr, Fe, Mn and Ni. This striking feature suggests that in contrast to the Fe/Al interface, the formation of the $Al_{13}(CoCrFeMnNi)_4$ layer at the CoCrFeMnNi/Al interface is fulfilled mainly by the diffusion of Al into CoCrFeMnNi.

The mixing enthalpy (ΔH_{mix}) values for Co–Al, Cr–Al, Fe–Al, Mn–Al and Ni–Al element pairs are − 19 kJ/mol, − 10 kJ/mol, − 11 kJ/mol, − 19 kJ/mol, and − 22 kJ/mol, respectively [49]. These negative values are normally clear indication of strong chemical affinity of each of the constituent elements with Al. As Al diffuses into the CoCrFeMnNi matrix, if each constituent element can undergo free long-range atomic migration, according to the phase diagrams [43] of the binary Co-Al, Cr–Al, Fe–Al, Mn-Al and Ni–Al systems, a large number of stable intermetallic compounds (such as Cr_2Al, Al_4Mn, Al_5Fe_2, $Al_{13}Fe_4$, Co_2Al_5, Ni_3Al and NiAl) could form. It is a surprise, however, that only one type of IMC ($Al_{13}(FeNiCoCrMn)_4$) is seen at the CoCrFeMnNi/Al interface. This is likely a result of the fact that the long-range atomic migration of the constituents is

suppressed by the compositional complexities which either causes greater fluctuation of lattice potential energy and thus higher activation energies or produces more traps/blocks for long-range atomic migration and thus lower atom mobility/diffusivity [29, 32, 33].

3.3 Diffusion Kinetics

A series of static diffusion experiments were performed to quantify the kinetics of diffusion at the CoCrFeMnNi/Al interface and compare with that at the Fe/Al interface. For each set of experiments, a single piece of Al was sandwiched between a Fe piece and a CoCrFeMnNi piece to simultaneously generate a Fe/Al interface and a CoCrFeMnNi/Al interface. This three-layer setup was placed inside a graphite die, and the diffusion experiments were performed using SPS with a temperature ranging from 550 to 625 °C and a holding time from 900 to 3600 s. For all tests, the axial pressure was kept at 30 MPa.

The interface IMC thickness measured from the BSE images is shown in Fig. 9 as a function of diffusion temperature and time. It is clear that under the same processing condition, the IMC layer thickness of the Fe/Al interface is dramatically thicker than that of the CoCrFeMnNi/Al interface. For example, after diffusion welding at 575 for 30 min, the thickness of the Fe/Al interface IMC is about 52.3 μm, while the CoCrFeMnNi/Al interface IMC is 8.7 μm. The following equation was used to calculate the growth rate constants:

$$x^2 = Dt$$

where x is the product layer thickness (μm), D is the interdiffusion coefficient or grow rate (m^2/s), and t is the diffusion time (s). The obtained interdiffusion coefficient of Fe/Al and CoCrFeMnNi/Al interface at different temperatures is shown in Fig. 10. Under the same condition, the interdiffusion coefficient at the Fe/Al interface is dramatically larger than that at the CoCrFeMnNi/Al interface. Specifically, at 600 ℃, the interdiffusion coefficient of Fe/Al interdiffusion and CoCrFeMnNi/Al interdiffusion is 1.5×10^{-11} m^2/s and 6×10^{-14} m^2/s, respectively. The following Arrhenius equation was applied to calculate the activation energy for the formation of the reaction layers (Fig. 10a):

$$\ln D = \ln D_0 + \frac{Q}{RT}$$

where Q is the activation energy for the formation of the intermetallic layers. D_0 is the constant, R is the universal gas constant, and T is the diffusion temperature. The activation energy for the formation of Fe/Al diffusion couple was calculated to be ~ 341.6 kJ/mol. This value is significantly higher than that for the same binary system without SPS (155–190 kJ/mol) [44, 50]. This phenomena can be attributed to the high pressure yielded by the pulse current in addition to the applied pressure [51, 52]. The activation energy obtained here is slightly higher than that obtained by Li et al. [45] (~ 332 kJ/mol) for the same Fe/Al binary system under SPS condition. This difference arises likely from the higher applied axial pressure (30 MPa) than that in Li et al. (5 MPa) [45].

It is noted that the activation energy for IMC formation at the CoCrFeMnNi/Al interface (~ 329.5 kJ/mol) is slightly

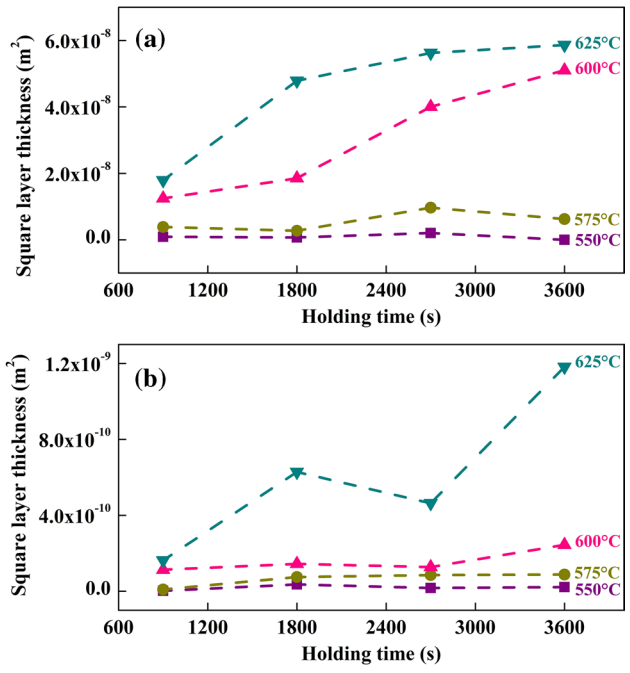

Fig. 9 Thickness of the IMC layers at **a** the Fe/Al and **b** the CoCrFeMnNi/Al interfaces obtained under different temperatures and annealing time

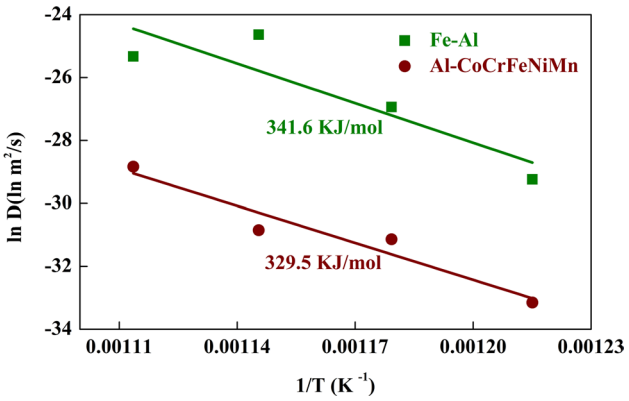

Fig. 10 Arrhenius plot of interdiffusion coefficient D as a function of temperature for the Fe/Al and CoCrFeMnNi/Al binary diffusion couples

lower than that at the Fe/Al interface (~ 341.6 kJ/mol). During the diffusion process, the interdiffusion coefficient was determined by two major factors, the diffusion activation energy and the atom diffusivity [53]. A higher activation energy for diffusion is normally prone to decreasing the diffusion coefficient. But, as stated above, under the same annealing conditions, the diffusion coefficient of Fe/Al diffusion couple is nearly a few tens of times that of the CoCrFeMnNi/Al diffusion couple. Thus, the reduced atom mobility/diffusivity instead of higher activation energy is the major contribution that causes the observed significantly lower interdiffusion coefficient at the CoCrFeMnNi/Al couple.

3.4 Insights into the Application of High-Entropy Alloys as "Interlayer" Materials for Al-Steel Dissimilar Metal Solid-State Joining

The above experimental findings showed the absence of IMC layer at the CoCrFeMnNi/Fe solid/solid interface. To positively assert that the CoCrFeMnNi alloy can be applied as "interlayer" materials for Al-steel solid-state joining, a complete avoidance of IMC formation at the CoCrFeMnNi/Al interface would be an ideal situation. But this is not achieved in the current study. Despite this, when CoCrFeMnNi/Al interface is exposed to solid/solid diffusion condition, the thickness of the formed IMC ($Al_{13}(CoCrFeMnNi)_4$) layer can be dramatically reduced. Besides the thickness of the IMC layer, another important criteria to assess its suitability for application is the brittleness of the IMC layer, which can be indirectly related to its hardness. Thus, to provide further insights, we measured the IMC nanohardness using nanoindentation under 50 mN normal load. The average hardness of the IMCs at the Fe/Al and CoCrFeMnNi/Al interfaces is 1049 HV and 888 HV, respectively, indicating a lower brittleness of the $Al_{13}(CoCrFeMnNi)_4$ at the CoCrFeMnNi/Al interface than that of the Al_5Fe_2 at the Fe/Al interface. In addition, to ensure a sound Al-steel joint with good mechanical properties, it is generally recognized that the critical limit for IMC layers is about 10 μm [10, 54]. From the above-shown experimental results, this critical condition is achievable. For example, when the CoCrFeMnNi/Al couple was annealed at 575 °C for 15 min, the obtained IMC layer exhibits a thickness of about 3.1 μm; this value can be further reduced down to about 1.5 μm when the annealing temperature is 550 °C.

Worth noting that the above-mentioned results are obtained from static binary diffusion experiments, during the practical solid-state Al-steel (e.g., friction stir) joining, the interface would experience much more complicated thermomechanical conditions. For example, during friction stir joining of Al alloys and HEA-coated steels, the HEA/Al weld interface would experience a peak temperature lower than 550 °C with a soaking time of seconds [55]; thus the formation of much thinner IMC layers can be expected. In addition to this, due to the effects of "stirring," the softened Al alloy matrix would experience severe plastic deformation and flow of materials. This will further complicate the nature of the weld interface. Two recent studies supported this speculation. Yao et al. [56] performed a phase identification for the interface formed during friction stir lap welding of the CoCrFeMnNi alloy to an Al alloy. Similar to the current observation, they reported the formation of $Al_{13}Fe_4$ phase with 1.3–1.7 μm thickness but the constituent elements (Co, Cr, Fe, Mn and Ni) no longer maintain their equiatomicity nature, with Cr and Mo significantly depleted. Nene et al. [57] friction stir butt-welded a $Fe_{30}Mn_{20}Co_{20}Cr_{15}Si_5Al_1$ HEA with a high-strength Al-7050 alloy and observed a complete avoidance of IMC formation.

The above findings and analysis suggest the possibility to obtain HEA/Al interface with reduced thickness and lower brittleness and indicate the potential of using HEAs as "interlayer" materials for Al-Steel solid-state joining. However, more systematical and extensive investigation on the effects of dynamic thermomechanical processing conditions and HEA composition on the IMC formation and the correlation between the characteristics (thickness, phase and composition) of IMC and the interface bonding strength are needed to verify this.

4 Summary and Conclusions

To shed light into the application potential of high-entropy alloys as "interlayer" materials for Al-steel solid-state joining, we investigated the nature of the CoCrFeMnNi/Fe and CoCrFeMnNi/Al interfaces, focusing on the bonding behavior and phase components. Based on the current study, the following conclusions can be drawn:

1. Good metallurgical bonding without the formation of hard and brittle IMC can be achieved at the CoCrFeMnNi/Fe solid/solid interface.
2. In contrast to the formation of Al_5Fe_2 phase at the Fe/Al interface, a $Al_{13}Fe_4$-type IMC dominates the CoCrFeMnNi/Al interface, and the Fe site in the IMC is co-occupied equally by Co, Cr, Fe, Mn and Ni.
3. Although the formation of IMC at the CoCrFeMnNi/Al interface is not avoidable, the thickness and hardness of the IMC formed at the interface can be largely reduced compared to that at the Fe/Al interface.
4. The activation energy for the interdiffusion of Fe/Al and CoCrFeMnNi/Al static diffusion couple is 341.6 kJ/mol and 329.5 kJ/mol, respectively. Despite this similarity, under identical static annealing condition, the interdiffusion coefficient of the CoCrFeMnNi/Al diffusion couple is significantly lower than that of the Fe/Al diffusion couple. This is mainly a result of the reduced atomic

mobility/diffusivity caused by the compositional complexity in the CoCrFeMnNi high-entropy alloy.

Acknowledgements This work was financially supported by the National Natural Science Foundation of China (No. 51901077), the Science and Technology Innovation Platform and Talent Plan of Hunan Province (Grant No. 2019RS1020), and the open Foundation of State Key Laboratory of Advanced Design and Manufacturing for Vehicle Body, Hunan University, Changsha, China (No. 71865003).

References

[1] J. Singh, K.S. Arora, D.K. Shukla, J. Alloys Compd. **783**, 753 (2019)
[2] J. Chen, Z. Feng, H. Wang, B.E. Carlson, T. Brown, D. Sigler, Mater. Sci. Eng. A **735**, 145 (2018)
[3] G. Qin, Z. Ao, Y. Chen, C. Zhang, P. Geng, J. Mater. Process. Technol. **273**, 116255 (2019)
[4] Y. Li, H. Ma, J. Wang, Mater. Sci. Eng. A **528**, 4343 (2011)
[5] G. Qin, Y. Su, S. Wang, Acta Metall. Sin. **48**, 1018 (2012)
[6] W. Lee, M. Schmuecker, U.A. Mercardo, G. Biallas, S.B. Jung, Scr. Mater. **55**, 355 (2006)
[7] H. Uzun, C.D. Donne, A. Argagnotto, T. Ghidini, C. Gambaro, Mater. Des. **26**, 41 (2005)
[8] T. Ogura, Y. Saito, T. Nishida, H. Nishida, T. Yoshida, N. Omichi, M. Fujimoto, A. Hirose, Scr. Mater. **66**, 531 (2012)
[9] Z. Shen, Y. Ding, J. Chen, B.S. Amirkhiz, J.Z. Wen, L. Fu, A.P. Gerlich, J. Mater. Sci. Technol. **35**, 1027 (2019)
[10] H. Springer, A. Kostka, E.J. Payton, D. Raabe, A. Kaysser-Pyzalla, G. Eggeler, Acta Mater. **59**, 1586 (2011)
[11] S. Bozzi, A.L. Helbert-Etter, T. Baudin, B. Criqui, J.G. Kerbiguet, Mater. Sci. Eng. A **527**, 4505 (2010)
[12] G.M. Reddy, A.S. Rao, T. Mohandas, Sci. Technol. Weld. Join. **13**, 619 (2008)
[13] J.W. Yeh, S.K. Chen, S.J. Lin, Adv. Eng. Mater. **6**, 299 (2004)
[14] Y. Zhang, T.T. Zuo, Z. Tang, M.C. Gao, K.A. Dahmen, P.K. Liaw, Z.P. Lu, Prog. Mater. Sci. **61**, 1 (2014)
[15] Z. Wu, H. Bei, G.M. Pharr, E.P. George, Acta Mater. **81**, 428 (2014)
[16] B. Gludovatz, A. Hohenwarter, D. Catoor, E.H. Chang, E.P. George, R.O. Ritchie, Science **345**, 1153 (2014)
[17] Z. Wu, H. Bei, F. Otto, G.M. Pharr, E.P. George, Intermetallics **46**, 131 (2014)
[18] Y. Lu, Y. Dong, S. Guo, L. Jiang, H. Kang, T. Wang, B. Wen, Z. Wang, J. Jie, Z. Cao, H. Ruan, T. Li, Sci. Rep. **4**, 6200 (2014)
[19] Z.J. Zhang, M.M. Mao, J. Wang, B. Gludovatz, Z. Zhang, S.X. Mao, E.P. George, Y. Qian, R.O. Ritchie, Nat. Commun. **6**, 10143 (2015)
[20] Y.F. Ye, Q. Wang, J. Lu, C.T. Liu, Y. Yang, Mater. Today **19**, 349 (2016)
[21] Z. Wu, Y. Gao, H. Bei, Acta Mater. **120**, 108 (2016)
[22] D.B. Miracle, O.N. Senkov, Acta Mater. **122**, 448 (2017)
[23] Z. Fu, L. Jiang, J.L. Wardini, B.E. Macdonald, H. Wen, W. Xiong, D. Zhang, Y. Zhou, T.J. Rupert, W. Chen, Sci. Adv. **4**, 8712 (2018)
[24] R. Zhang, S. Zhao, J. Ding, Y. Chong, T. Jia, C. Ophus, M. Asta, R.O. Ritchie, A.M. Minor, Nature **581**, 283 (2020)
[25] N. Jia, Y. Li, H. Huang, S. Chen, D. Li, Y. Dou, X. He, W. Yang, Y. Xue, K. Jin, J. Nucl. Mater. **552**, 152937 (2021)
[26] Y. Dong, S. Chen, N. Jia, Q. Zhang, L. Wang, Y. Xue, K. Jin, Tungsten (2021). https://doi.org/10.1007/s42864-021-00111-8
[27] X. Li, Z. Li, Z. Wu, S. Zhao, W. Zhang, H. Bei, Y. Gao, J. Mater. Sci. Technol. **94**, 264 (2021)
[28] D. Li, Y. Dong, Z. Zhang, Q. Zhang, S. Chen, N. Jia, H. Wang, B. Wang, K. Jin, Y. Xue, Y. Dou, X. He, W. Yang, L. Wang, H. Cai, J. Alloys Compd. **877**, 160190 (2021)
[29] W. Li, D. Xie, D. Li, Y. Zhang, P.K. Liaw, Prog. Mater. Sci. **118**, 100777 (2021)
[30] D.B. Miracle, J.D. Miller, O.N. Senkov, C. Woodward, M.D. Uchic, J. Tiley, Entropy **16**, 494 (2014)
[31] J.W. Yeh, Ann. Chim. Sci. Mat. **31**, 633 (2006)
[32] K.Y. Tsai, M.H. Tsai, J.W. Yeh, Acta Mater. **61**, 4887 (2013)
[33] M. Vaidya, K.G. Pradeep, B.S. Murty, G. Wilde, S.V. Divinski, Acta Mater. **146**, 211 (2018)
[34] B.X. Cao, C. Wang, T. Yang, C.T. Liu, Scr. Mater. **187**, 250 (2020)
[35] G.M. Karthik, S. Panikar, G.D.J. Ram, R.S. Kottada, Mater. Sci. Eng. A **679**, 193 (2017)
[36] T. Lu, S. Scudino, W. Chen, P. Wang, D. Li, M. Mao, L. Kang, Y. Liu, Z. Fu, Mater. Sci. Eng. A **726**, 126 (2018)
[37] G. Meng, X. Lin, H. Xie, C. Wang, S. Wang, X. Ding, J. Alloys Compd. **672**, 660 (2016)
[38] W. Chen, Z. Li, T. Lu, T. He, R. Li, B. Li, B. Wan, Z. Fu, S. Scudino, Mater. Sci. Eng. A **762**, 138116 (2019)
[39] B. Cantor, Prog. Mater. Sci. **120**, 100754 (2021)
[40] J. Li, X. Meng, L. Wan, Y. Huang, J. Manuf. Process. **68**, 293 (2021)
[41] N.K. Adomako, G. Shin, N. Park, K. Park, J.H. Kim, J. Mater. Sci. Technol. **85**, 95 (2021)
[42] W. Ding, N. Liu, J. Fan, J. Cao, X. Wang, Intermetallics **129**, 107027 (2021)
[43] T.B. Massalski, H. Okamoto, P.R. Subramanian, L. Kacprzak, Binary Alloy Phase Diagrams, (ASM International, Materials Park, 1990), vol. 1, p.147
[44] D. Naoi, M. Kajihara, Mater. Sci. Eng. A **459**, 375 (2007)
[45] R. Li, T. Yuan, X. Liu, K. Zhou, Scr. Mater. **110**, 105 (2016)
[46] K. Hirano, R.P. Agarwala, M. Cohen, Acta Metall. **10**, 857 (1962)
[47] R.P. Agarwala, S.P. Murarka, M.S. Anand, Acta Metall. **12**, 871 (1964)
[48] S. Fujikawa, K.I. Hirano, Mater. Sci. Forum **13**, 539 (1987)
[49] A. Takeuchi, A. Inoue, Mater. Trans. **46**, 2817 (2005)
[50] V. Jindal, V.C. Srivastava, A. Das, R.N. Ghosh, Mater. Lett. **60**, 1758 (2006)
[51] G. Chiu, A. Ng, Phys. Rev. E **59**, 1024 (1999)
[52] K. Oh-ishi, K. Edalati, H.S. Kim, K. Hono, Z. Horita, Acta Mater. **61**, 3482 (2013)
[53] D.A. Porter, K.E. Easterling, *Phase Transformations in Metals and Alloys* (Chapman and Hall, London, 1992)
[54] D.R.G. Achar, J. Ruge, S. Sundaresan, Aluminium **56**, 220 (1980)
[55] P. Kaushik, D.K. Dwivedi, J. Manuf. Process. **68**, 198 (2021)
[56] H. Yao, H. Wen, K. Chen, M. Jiang, K.M. Reddy, K. Kondoh, M. Wang, X. Hua, A. Shan, Scr. Mater. **201**, 113972 (2016)
[57] S. Nene, S. Gupta, C. Morphew, R.S. Mishra, Materialia **11**, 100740 (2020)